2008 IEEE International Conference on
Robotics and Automation
Pasadena, CA, USA, May 19-23, 2008

Design of a Planar Robotic Machine for Neuro-rehabilitation

Loredana Zollo, Dino Accoto, Francesco Torchiani, Domenico Formica, Eugenio Guglielmelli

Abstract— **This paper presents the design criteria of a robot manipulator for the rehabilitation of the upper limb. The machine is conceived to optimize the dynamic behavior in the interaction with the patient, basically in terms of low impedance when back-driven and low and isotropic inertial properties.**

Robot kinematics and dynamics are mathematically modeled and its dynamic properties are measured in the workspace in terms of inertia and acceleration capabilities. A method is used that is borrowed from the literature and is based on inertia and acceleration graphical representation through ellipsoids.

I. INTRODUCTION

The design of a robotic machine for robot-aided neuro-rehabilitation develops in a highly collaborative research scenario where roboticists, neuroscientists and medical doctors contribute to define system specifications. The main reason is that the human subject (i.e. the patient exposed to the rehabilitation therapy) plays a key-role in the design in view of the tight and continuous physical human-robot coupling [1]. Robot-mediated therapy enables even severely impaired patients to play a key active role in the execution of a motor task. The robot helps the subject to carry out the part of the task that she/he is not able anymore to perform autonomously, with a level of assistance that can be adapted to her/his residual abilities. Requirements like extreme accuracy, repeatability, pre-programmed movements and task specificity (typical of industrial or service robots [2], [3]) undergo the priority features imposed by the close physical contact with the user, such as safety, reliability, robustness, adaptability, mechanical reversibility (back-driveability), which are strongly dependent on the robot mechanical and control design [4], [5], [6].

Several examples of robotic machines for rehabilitation can be found in the literature [7], [8], [9], [10], [11], [12], [13], [14], [15], [16], [17]. However, most of these systems share the common approach of adapting or re-configuring industrial robots for use in rehabilitation with the consequent critical drawback that low impedance comparable to the human arm cannot practically be obtained, being the machines intrinsically position-controlled. Despite the use of active force feedback to enhance robot responsiveness, "back-driveability" (low mechanical impedance) required to move smoothly and rapidly in compliance with a patient's actions [18] is not achieved. High inertia, anisotropy of dynamic properties and low acceleration capabilities are often the main responsible for that [19], [20]. On the other hand, meaningful examples of back-driveable systems are the haptic interfaces, which are designed in order to make the user perceive a very low mass [21].

L. Zollo, D. Accoto, F. Torchiani, D. Formica, E. Guglielmelli are with Biomedical Robotics and Biomicrosystems, Università Campus Bio-Medico, via Alvaro del Portillo 21, 00128 Roma, Italy ({l.zollo, d.accoto, d.formica, e.guglielmelli}@unicampus.it)

Based also on our experience in robot-aided neuro-rehabilitation, we are currently developing a planar robot for the upper limb rehabilitation (named CBM-Motus) which tries to go beyond the current state of the art in terms of low and isotropic inertia when back-driven. In other words, our purpose is to design a robot having inertia ellipses with small radius and unitary eccentricity, which are independent on the robot configuration in the workspace [22], [23].

In this paper the design criteria for such a machine are presented, as well as the study of its dynamic properties through inertial and acceleration ellipsoids. The method, borrowed from previous works on the dynamic optimization of robot design [22], [24], allows studying the robot inertia and acceleration characteristics as perceived at the end effector.

The results have been compared with the dynamic features of other machines, in particular the Mit-manus system that is the robotic machine for the rehabilitation of the upper limb [25] currently available in our laboratory and used in clinical applications with post-stroke patients [17], [26], [27].

II. DESIGN OF THE CBM-MOTUS ROBOT

The design criteria of the CBM-motus have been inspired by the need of achieving:

- high back-driveability (low friction; low and isotropic apparent inertia when back-driven);
- a large workspace to allow the subministration of several rehabilitative treatments (target: $> 500\ mm \times 500\ mm$);
- interaction forces up to $50\ N$.

The kinematic structure of the CBM-motus is based on two identical modules connected by a double prismatic joint, as it will be shown soon. A module comprises six pulleys having the same radius ($25\ mm$) and two belts (Fig. 1). Two couples of pulleys (on the left in Fig. 1) are mounted on the same shafts. One pulley per module is connected to the driving motor. Two belts for each module are mounted in such a way that the points along the segments AB and CD move vertically with the same speed. A transmission bar is fixed to a couple of such points, e.g. P and P' in Fig. 1. The bar allows the movements of the end-effector along the y direction. By supporting both bar ends, a good rigidity can be achieved with an overall mass saving if compared to the conventional solution where one bar end is connected to the driving belt and the other one is simply supported by a linear slider.

The second module is mounted over the first one with a rotation of $90°$ around the z-axis. The bar in the second

module allows the displacements of the end-effector along the x-direction. The motion of the two bars is transmitted to the end-effector, i.e. to the handle of the robot, by a joint obtained by rigidly linking two prismatic joints with orthogonal axes.

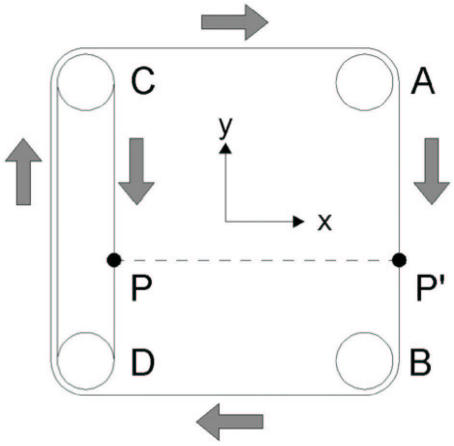

Fig. 1. Schematic of a single kinematic module comprising 6 pulleys and 2 belts. P and P' move vertically with the same speed.

The schematic of the kinematics of the CBM-motus is shown in Fig. 2. The outer prismatic joints $(P_1, \ldots, P_4)$ correspond to the segments of the belts to which the two bars (1 and 2) are connected. The two bars slide through a compound prismatic joint $(A+B)$, to which the end-effector (E) is connected. The bars and the double prismatic joint are depicted in Fig. 3.

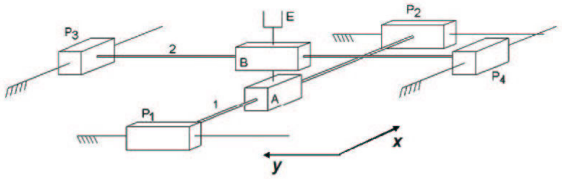

Fig. 2. CBM-motus kinematic scheme.

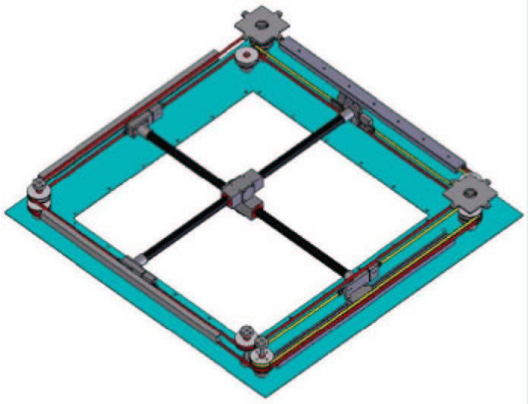

Fig. 3. Overview of the two assembled kinematic modules. The rigid bars slide in a double prismatic joint and are connected to the driving belts.

The two bars sliding in the double prismatic joint are connected to the transmission belts (timing belt XL037, $9.4\ mm$ wide, reinforced with a glass fiber cord for improved inextensibility). This may result in a low stiffness of the robot in the case the belts are bent instead of stretched. But note that the double-prismatic joint assures that only stretching (tensile) forces are transmitted to the belts. In fact, each joint can transmit to the bar sliding through it only the force component which is orthogonal to the same bar, while free sliding is permitted along the direction of the axis. In this way each bar stretches the belts it is connected to, without bending. Nevertheless, each prismatic joint is not ideally frictionless, so that small axial forces due to friction may be produced during the sliding. Such spurious forces, which might cause a slight bending of the belts, are counterbalanced by linear sliders mounted orthogonally to the bars and also connected to the transmission belts. By blocking any transverse movement, the sliders assure a high stiffness of the transmission. This feature, together with the low mass of the belts, assure a high resonance frequency, which is necessary to avoid spurious mechanical stimuli during the haptic rendering. In addition, the resonance frequency can be manually tuned during assembly by regulating the pretension of the belts. Note that the chosen timing belts and pulleys, thanks to their good kinematic coupling, assure a smooth, almost noiseless motion, with no perceivable vibrational effect due to cogs.

Vertical loads (i.e. along the z-axis) are counterbalanced by a ball bearing located between the double joint and the bottom of the frame. Bars have been dimensioned so that their flexural stiffness limits the maximum linear and rotary deflections within the range of tolerance of the linear joints, when the maximum interaction force is applied to the handle, including the weight of the forearm possibly supported by a splint connected to the handle of the CBM-Motus. Based on experimental results to be obtained on the prototype, the possibility of supporting the patient's forearm using an external device (e.g. forearm supported by belts connected by a vertical rigid link clamped to the frame) will be taken into account in order to further reduce the deflection of the beams.

The two modules are actuated using DC servomotors fixed to the frame (Aerotech BM 250) with rated torque of $2\ Nm$ and peak torque of $5\ Nm$. Being $R = 25\ mm$ the radius of the pulleys, the maximum force which the robot is able to exert is $80\ N$ (peak force: $200\ N$). The planar workspace is square in shape with a side of $550\ mm$. The overall dimensions of the robot frame are $830 \times 820 \times 110\ mm$. The total mass (frame and motors included) is about $30\ kg$. The overview of the system is shown in Fig. 4.

The CBM-Motus robot can be regarded as a Cartesian manipulator with two linear joints d_1 and d_2. The robot kinematics (Fig. 2) is very easy being

$$\begin{bmatrix} x \\ y \end{bmatrix} = \begin{bmatrix} d_1 \\ d_2 \end{bmatrix} \tag{1}$$

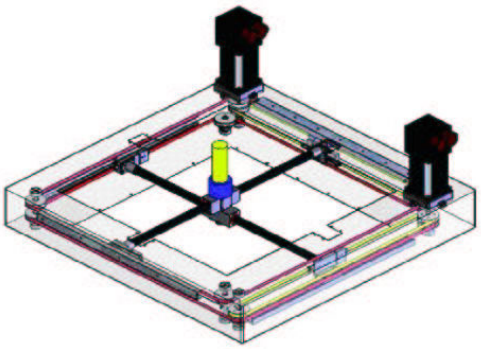

Fig. 4. Overview of the complete robot.

the forward kinematics to compute the end-effector Cartesian position and

$$J = \begin{bmatrix} z_0 & z_1 \end{bmatrix} = \begin{bmatrix} 1 & 0 \\ 0 & 1 \end{bmatrix} \tag{2}$$

the Jacobian matrix.

The Lagrangian formulation is used to derive the robot dynamic model. Thus, consider the following Lagrangian equations

$$\frac{d}{dt}\frac{\partial L}{\partial \dot{q}_i} - \frac{\partial L}{\partial q_i} = \tau_i \qquad i{=}1{,}2 \tag{3}$$

where $L = T - U$ is the difference between system kinetic energy T and potential energy U, $q_i = d_i$ and τ_i is the joint torque. Consider that, due to the planar structure of the robot, the gravitational energy is structurally compensated and L effectively includes only the kinetic energy expressed as

$$T = \frac{1}{2}m_{l1}\dot{d}_1^2 + \frac{1}{2}m_{l2}\dot{d}_2^2 + \frac{1}{2}I_{m1}\dot{d}_1^2/R^2 + \frac{1}{2}I_{m2}\dot{d}_2^2/R^2. \tag{4}$$

In (4) m_{l1} and m_{l2} (with $m_{l1} = m_{l12}$) indicate the translating masses, including bars, belts and handle; $\omega_{m1} = \frac{\dot{d}_1}{R}$ and $\omega_{m2} = \frac{\dot{d}_2}{R}$ are the angular motor velocities; $I_{m1} = I_m + 6I_p$ and $I_{m2} = I_{m1} = I_m$ are the moments of inertia due to the two motors (I_m) and the twelve pulleys (I_p); R is the pulley radius.

By resolving eqs. (3) the following robot dynamic model is obtained:

$$B(q)\ddot{q} + c(q,\dot{q}) + F_v\dot{q} = \tau, \tag{5}$$

being

$$B = \begin{bmatrix} m_{l1} + I_{m1}/R^2 & 0 \\ 0 & m_{l2} + I_{m2}/R^2 \end{bmatrix} \tag{6}$$

the inertia matrix (independent on the robot configuration), $c(q,\dot{q}) = \begin{bmatrix} 0 & 0 \end{bmatrix}^T$ the vector of centrifugal and Coriolis torques, and $F_v\dot{q}$ the viscous friction torque with $f_{vii} = 1.53$ Ns.

III. Inertia and Acceleration Ellipsoids

The study of the CBM-Motus dynamic properties has been carried out through the estimation of the robot inertial and acceleration capabilities in the workspace and their spatial representation through ellipsoids. The approach is resumed from [22], [23], [24] and is briefly presented here in order to explain its application to the designed robotic machine. However, further details on the mathematical formulation can be found in [22], [23], [24].

A. Inertia Ellipsoids

Consider the robot dynamic model in the operational space expressed as

$$\Lambda(q)\dot{\theta} + \mu(q,\dot{q}) + p(q) = F \tag{7}$$

where

$$\Lambda^{-1}(q) = J(q)B^{-1}(q)J^T(q) \tag{8}$$

$\mu(q,\dot{q})$, $p(q)$, F are the centrifugal and Coriolis force vector, the gravity force vector and the generalized force vector acting in the operational space, respectively, and

$$\theta = \begin{bmatrix} v \\ \omega \end{bmatrix} = J(q)\dot{q} = \begin{bmatrix} J_v \\ J_\omega \end{bmatrix}\dot{q}.$$

Matrix $\Lambda(q)$ is the *generalized inertia tensor* [22] of a series of rigid bodies and the equation

$$u^T\Lambda u \tag{9}$$

describes a *generalized inertia ellipsoid* (GIE) having the following properties:

- the principal axes are aligned with Λ eigenvectors $\lambda(\Lambda)$;
- the length of each principal axis is $\frac{1}{\sqrt{\lambda(\Lambda)}}$.

By separating linear and angular contributions, the generalized inertia matrix can also be written as

$$\Lambda^{-1} = \begin{bmatrix} \Lambda_v^{-1}\overline{\Lambda}_{v\omega} \\ \overline{\Lambda}_{v\omega}^T\Lambda_\omega^{-1} \end{bmatrix} \tag{10}$$

where $\Lambda_v(q)$ is homogeneous to a mass matrix, $\Lambda_\omega(q)$ is homogeneous to an inertia matrix, and $\overline{\Lambda}_{v\omega}(q)$ provides a description of the coupling between translational and rotational motion.

Given $\Lambda(q)$ as in (10), the inertial features of the robot design can be estimated through

1. $\|\Lambda_v\|$ and $\|\Lambda_\omega\|$, which describe magnitude of inertial properties (the robot design tends to minimize them)
2. $k(\Lambda_v)$ and $k(\Lambda_\omega)$ (where $k(\cdot)$ is the matrix condition number), which describe the extent of isotropicity of the inertial properties (when $k(\Lambda_v) = 1$ and $k(\Lambda_\omega) = 1$ robot inertia is isotropic).

B. Acceleration Ellipsoids

Joint torques τ responsible for the robot motion can be extracted from (7) as

$$J^T \left(\Lambda \dot{\theta} + \mu \right) + g = \tau. \tag{11}$$

Given the torque boundary condition

$$-\tau_{bound} \leq \tau \leq \tau_{bound} \tag{12}$$

where τ_{bound} is the vector of maximum actuator torques, eq. (11) leads to

$$\tau_{lower} \leq \begin{bmatrix} E_v & E_\omega \end{bmatrix} \begin{bmatrix} \dot{v} \\ \dot{\omega} \end{bmatrix} + \begin{bmatrix} \theta^T M_1 \theta \\ \vdots \\ \theta^T M_n \theta \end{bmatrix} \leq \tau_{upper} \tag{13}$$

where N denotes matrix $N = diag\{\ldots, \frac{1}{\tau_{bound_i}}, \ldots\}$ and

$$\tau_{lower} = -1 - Ng \qquad \tau_{upper} = 1 - Ng \tag{14}$$

$$\begin{bmatrix} E_v & E_\omega \end{bmatrix} = NJ^T \Lambda \tag{15}$$

$$\begin{bmatrix} \theta^T M_1 \theta \\ \vdots \\ \theta^T M_n \theta \end{bmatrix} = NJ^T \mu.$$

The torque ellipsoid for linear acceleration is described by

$$\tau_v^T \left(E_v E_v^T \right)^\dagger \tau_v = a^2 = \|\dot{v}\|^2 \tag{16}$$

being

$$\dot{v}^T \dot{v} = a^2 \tag{17}$$

the acceleration hyper-sphere and

$$\tau_v = E_v \dot{v}$$

$$E_v^\dagger \tau_v = \dot{v}.$$

The ellipsoid is described by the core matrix $\left(E_v E_v^T \right)^\dagger$, where $E_v^\dagger = \left(E_v^T E_V \right)^{-1} E_v^T$ is the right pseudo-inverse matrix of E_v.

The torque ellipsoid for angular acceleration is obtained with analogous considerations (for details see [24]).

Robot acceleration capabilities can be evaluated by means of

1. $\|E_v\|$ and $\|E_\omega\|$, which measure magnitude of acceleration capability (minimizing them means to maximize acceleration)
2. $k(E_v)$ and $k(E_\omega)$, which measure isotropicity of acceleration capabilities, as for the inertia.

Mapping a sphere into the hyper-cube defined by the torque bounds is the best possible situation as an isotropic acceleration capability is achieved while most of the available actuator torque capability is used.

IV. CBM-Motus dynamic analysis

The following three main phases may be delineated for the dynamic study of the CBM-Motus robot:

1) Robot kinematic and dynamic modelling: only matrices Λ_v and E_v are calculated, being the robots planar.
2) Selection of a rehabilitation task covering a meaningful portion of the robot workspace: the clock task shown in Fig. 5 is chosen [26], as typically used for motor rehabilitation therapy.
3) Extraction of inertial and acceleration parameters and graphical visualization of the ellipses.

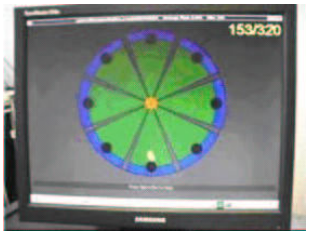

Fig. 5. Graphical interface for the rehabilitation clock exercise.

An analogous approach has been followed for the Mit-Manus robot available in our lab. Kinematic and dynamic models of the robot have been developed. Results from the dynamic analysis have been used as a benchmark for our inertial measures in addition to data gathered from the literature on haptic interface. For the Phantom, for example, from the literature it emerges that the user perceives no more than 100 grams of mass at the interface [21].

A. Inertial properties

Let Λ_{vMIT} and Λ_{vMotus} denote the inertial matrices in the operational space for the MIT-Manus and the CBM-Motus respectively. The analysis of the two robots in terms of inertial properties is based on the graphical representation of the ellipses given by eq. (9) and the estimation of the parameters $\|\Lambda_{vMIT}\|$ and $\|\Lambda_{vMotus}\|$ and $k(\Lambda_{vMIT})$ and $k(\Lambda_{vMotus})$.

Figures 6 and 7 show the inertia ellipses for the Mit-Manus and the CBM-Motus, respectively, in the nine Cartesian positions (P_1,.., P_9) that the robots reach while performing the rehabilitation clock task. Moreover, Tables I and II report the values of the Mit-Manus and CBM-Motus inertial parameters in the nine points. The inertia values calculated for the Mit-Manus are different with respect to those reported in the literature ([14]). The reason is that they have been extracted from the dynamic model of the new version of the machine, that was redesigned in order to host the wrist robot [28].

The inertia matrix for the CBM-Motus is independent on the robot configuration. Thus, the mass perceived at the end effector has the same value everywhere in the workspace and is given by 2.59 Kg. Also, the CBM-Motus is isotropic ($k(\Lambda_{vMotus}) = 1$). On the other hand, the Mit-Manus robot has maxima anisotropy in P_2 with a corresponding value of maxima mass of 4.48 Kg. The graphical representation through ellipses also allows identifying the direction of maxima inertia, that is given by the minor axis.

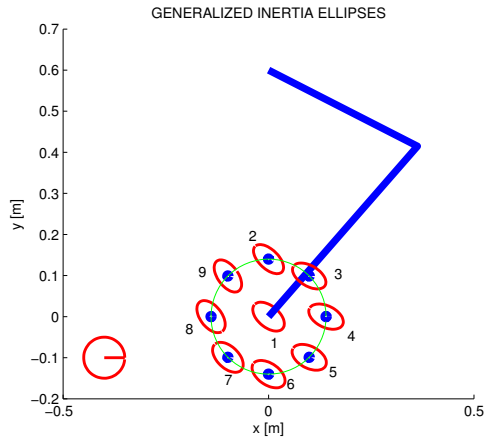

Fig. 6. Inertia ellipses for the Mit-Manus robot during the rehabilitation clock exercise.

	P1	P2	P3	P4	P5	P6	P7	P8	P9
$k(\Lambda_{vMIT})$	2.99	3.66	3.32	2.95	2.89	2.93	2.89	2.95	3.32
$\|\Lambda_{vMIT}\|$	3.68	4.48	4.08	3.64	3.57	3.62	3.57	3.64	4.08

TABLE I

INERTIA PARAMETERS FOR THE MIT-MANUS ROBOT DURING THE CLOCK EXERCISE

B. Acceleration properties

Let E_{vMIT} and E_{vMotus} denote the acceleration matrices in (15) for the MIT-Manus and the CBM-Motus, respectively, and eq. (16) describe the corresponding torque ellipse.

Similarly to the inertia analysis, Figs. 8 and 9 show the torque ellipses in the nine positions of the clock task, while Tables III and IV report the acceleration parameters $\|E_{vMIT}\|$, $\|E_{vMotus}\|$ and $k\left(E_{vMIT}\right)$, $k\left(E_{vMotus}\right)$ for measuring the magnitude of the acceleration properties and the level of isotropy of the Mit-Manus and the CBM-Motus.

Again, the Mit-Manus is anisotropic with a maximum in P_2 (where $k\left(E_{vMIT}\right)$ is 2.51 and $\|E_{vMIT}\|$ is 0.113 s^2), while the CBM-Motus is isotropic ($k\left(E_{vMotus}\right) = 1$) with a constant value of $\|E_{vMotus}\| = 0.52$ s^2. The direction of maxima acceleration is aligned with the ellipse minor axis and is given by 8.9 m/s^2 for the Mit-Manus and by 2.7 m/s^2 for the CBM-Motus. These values satisfy the condition of tangency with the square of torque bounds, being 14 Nm the torque bound for the Mit-Manus and 5 Nm the bound for the CBM-Motus.

V. CONCLUSIONS

This paper has presented the design of a planar robot for rehabilitation of the upper limb with low and isotropic inertia. The machine has been kinematically and dynamically

	P1	P2	P3	P4	P5	P6	P7	P8	P9
$k(\Lambda_{vMotus})$	1	1	1	1	1	1	1	1	1
$\|\Lambda_{vMotus}\|$	2.59	2.59	2.59	2.59	2.59	2.59	2.59	2.59	2.59

TABLE II

INERTIA PARAMETERS FOR THE CBM-MOTUS ROBOT DURING THE CLOCK EXERCISE

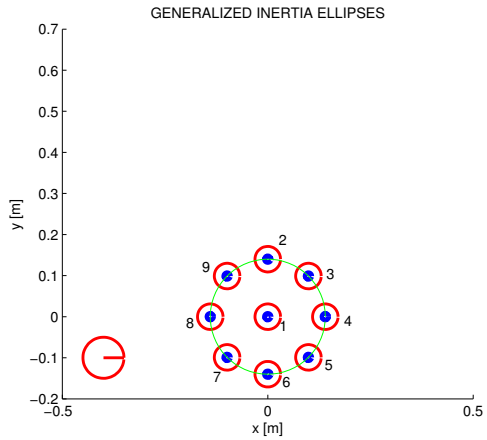

Fig. 7. Inertia ellipses for the CBM-Motus robot during the rehabilitation clock exercise.

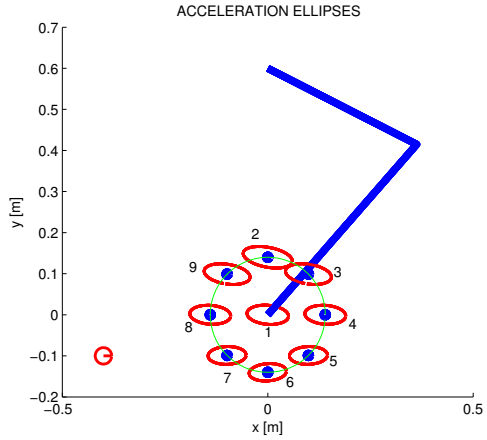

Fig. 8. Torque ellipses due to acceleration for the Mit-Manus robot during the rehabilitation clock exercise.

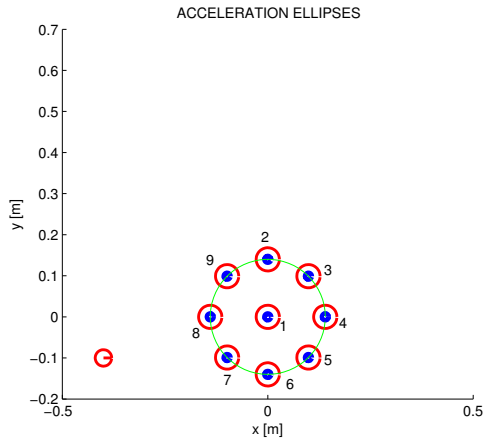

Fig. 9. Torque ellipses due to acceleration for the CBM-Motus robot during the rehabilitation clock exercise.

	P1	P2	P3	P4	P5	P6	P7	P8	P9
$k(E_{vMIT})$	2.20	2.51	2.36	2.17	2.14	2.17	2.14	2.17	2.36
$\|E_{vMIT}\|$	0.105	0.113	0.109	0.105	0.104	0.104	0.104	0.105	0.109

TABLE III

ACCELERATION PARAMETERS FOR THE MIT-MANUS ROBOT DURING THE CLOCK EXERCISE

	P1	P2	P3	P4	P5	P6	P7	P8	P9
$k(E_{vMotus})$	1	1	1	1	1	1	1	1	1
$\|E_{vMotus}\|$	0.52	0.52	0.52	0.52	0.52	0.52	0.52	0.52	0.52

TABLE IV

ACCELERATION PARAMETERS FOR THE CBM-MOTUS ROBOT DURING THE CLOCK EXERCISE

modeled. Then, a dynamic characterization in terms of inertia and acceleration ellipsoids has been carried out. This study has demonstrated that the main purpose of low inertia and isotropy of dynamic properties has been achieved. However, the equivalent mass at the end effector has to be further reduced for addressing applications as haptic interface. In addition, the robot shows reduced acceleration capabilities with respect to the Mit-Manus system, that future work will try to improve.

Future efforts will be addressed to analyze the frictional properties of the robot and the effects of belts compliance on the control. Thus, the design of the control system, the experimental validation of the machine and the development of an interactive interface for the therapist and the patient will be developed. The clinical application is finally envisaged for an extensive use of the machine with neurological patients (such as chronic post-stroke, inpatients, brain injured people).

REFERENCES

[1] D. Reinkensmeyer, N. Hogan, H.I. Krebs, S.L. Lehman, P.S. Lum, "Rehabilitators, Robots and Guides: New Tools for Neurological Rehabilitation", In: *Biomechanics and Neural Control of Posture and Movement*, J. Winters and P. E. Crago, Eds. Springer-Verlag, Berlin, pp. 516534, 2000.

[2] B. Siciliano, L. Villani, *Robot Force Control*, Kluwer Academic, Boston, 1999.

[3] D.M. Gorinevsky, A.M. Formalsky, A.Y. Schneider, *Force Control of Robotics Systems*, CRC Press, Boca Raton, 1997.

[4] L. Zollo, B. Siciliano, C. Laschi, G. Teti, P. Dario, "An Experimental Study on Compliance Control for a Redundant Personal Robot Arm", Rob. Auton. Syst., 44, pp. 101129, 2003.

[5] D. Formica, L. Zollo, E. Guglielmelli, "Torque-dependent Compliance Control in the Joint Space of an Operational Robotic Machine for Motor Therapy", *ASME Journal of Dynamic Systems, Measurement, and Control*, 2006, vol. 128, pp. 152–158.

[6] L. Zollo, B. Siciliano, A. De Luca, E. Guglielmelli, P. Dario, "Compliance control for an anthropomorphic robot with elastic joints: Theory and experiments", *ASME Journal of Dynamic Systems, Measurement, and Control*, 2005, vol. 127, pp. 321–328.

[7] D.J. Reinkensmeyer, L.E. Kahn, M. Averbuch, A. McKenna-Cole, B.D. Schmit, W.Z. Rymer, "Understanding and treating arm movement impairment after chronic brain injury: progress with the ARM guide", *Journal of Rehabilitation Research and Development*, vol. 37, pp. 653-662, 2000.

[8] L.E. Kahn, M. Averbuch, W.Z. Rymer, D.J. Reinkensmeyer, "Comparison of robot-assisted reaching to free reaching in promoting recovery from chronic stroke", in *Integration of assistive technology in the information age*, Mokhtari M Ed., IOS Press, Amsterdam (the Netherlands), pp. 39-44, 2001.

[9] R. Colombo, F. Pisano, S. Micera, A. Mazzone, C. Delconte, M.C. Carrozza, P. Dario, G. Minuco, "Upper limb rehabilitation and evaluation of stroke patients using robot-aided techniques", *Proceedings of the 9th International Conference on Rehabilitation Robotics*, Chicago, Illinois, pp. 515-518, 2005.

[10] S. Micera, M.C. Carrozza, E. Guglielmelli, G. Cappiello, F. Zaccone, C. Freschi, R. Colombo, A. Mazzone, C. Delconte, F. Pisano, G. Minuco, P. Dario, A Simple Robotic System for Neurorehabilitation, Autonomous Robots, vol. 19, pp. 271–284, 2005.

[11] C.G. Burgar, P.S. Lum, P.C. Shor, M. Van der Loos, "Development of robots for rehabilitation therapy: the Palo Alto VA/Stanford experience", *Journal of Rehabilitation Research and Development*, vol. 37, pp. 663-73, 2000.

[12] P. Lum, D.J. Reinkensmeyer, R. Mahoney, W.Z. Rymer, C. Burgar, "Robotic devices for movement therapy after stroke: current status and challenges to clinical acceptance", *Top Stroke Rehabilitation*, vol. 8, pp. 40–53, 2002.

[13] P.S. Lum, E. Taub, D. Schwandt, M. Postman, P. Hardin, G. Uswatte, "Automated Constraint-Induced Therapy Extension (AutoCITE) for movement deficits after stroke", *Journal of Rehabilitation Research and Development*, vol. 41, pp. 249-258, 2004.

[14] H.I. Krebs, N. Hogan, M.L. Aisen, B.T. Volpe, "Robot-aided neurorehabilitation", *IEEE Transactions on Rehabilitation Engineering*, vol. 6, pp. 75-87, 1998.

[15] B.T. Volpe, H.I. Krebs, N. Hogan, L. Edelstein, C. Diels, M. Aisen, "A novel approach to stroke rehabilitation: robotaided sensorimotor stimulation", *Neurology*, vol. 54, pp. 1938-1944, 2000.

[16] K. Kiguchi, K. Iwami, M. Yasuda, K. Watanabe, "An exoskeletal robot for human shoulder joint motion assist", *IEEE/ASME Trans. on Mechatronics*, vol. 8, pp. 125–135, 2003.

[17] G.B. Prange, M.J.A. Jannink, C.G.M. Groothuis-Oudshoorn, H.J. Hermens, M.J. IJzerman, "Systematic review of the effect of robot-aided therapy on recovery of the hemiparetic arm after stroke", *Journal of Rehabilitation Research and Development*, vol. 43, pp. 171-184, 2006.

[18] D.A. Lawrence, "Impedance control stability properties in common implementations", *Proceedings of the IEEE International Conference of Robotics and Automation*, pp. 1185–1191, 1988.

[19] C.S. Cai, B. Roth, "On the spatial motion of a rigid body with point contact", IEEE International Conference on Robotics and Automation, pp. 686–695, 1987.

[20] A. Sharon, N. Hogan, D.E. Hardt, "The Macro/Micro Manipulator: An Improved Architecture for Robot Control", *IEEE Transactions on Robotics and Automation*, 1988.

[21] T.H. Massie, J. K. Salisbury, "The PHANTOM Haptic Interface: A Device for Probing Virtual Objects", *Proceedings of the ASME Winter Annual Meeting, Symposium on Haptic Interfaces for Virtual Environment and Teleoperator Systems*, Chicago, IL, 1994.

[22] H. Asada, "Dynamic analysis and design of robot manipulators using inertia ellipsoids", *IEEE International Conference on Robotics*, Atlanta, pp. 94–102, 1984.

[23] O. Khatib, "Inertial properties in robotic manipulation: an object-level framework", *International Journal of Robotics Research*, vol. 14, pp. 19–36, 1995.

[24] O. Khatib, A. Bowling, "Optimization of the inertial and acceleration characteristics of manipulators", *IEEE International Conference on Robotics and Automation*, Minneapolis, MN, USA, pp. 2283–2289, 1996.

[25] N. Hogan, H.I. Krebs, A. Sharon, J. Charnnarong, "Interactive robotic therapist", Massachusetts Inst. Technol., Cambridge, U.S. Patent #5466213, 1995.

[26] S.E. Fasoli, H.I. Krebs, J. Stein, W.R. Frontera, R. Hughes, N. Hogan, "Robotic therapy for chronic motor impairments after stroke: follow-up results", *Arch Phys Med Rehabil*, vol. 85, pp. 1106–1111, 2004.

[27] M. Ferraro, J.J. Palazzolo, J. Krol, H.I. Krebs, N. Hogan, B.T. Volpe, "Robot-aided sensori-motor arm training improves outcome in patients with chronic stroke", *Neurology*, vol. 61, pp. 1604–1607, 2003.

[28] H.I. Krebs, B.T. Volpe, D. Williams, J. Celestino, S.K. Charles, D. Lynch, N. Hogan, "Robot-Aided Neurorehabilitation: A Robot for Wrist Rehabilitation", *IEEE Transactions on Neural Systems and Rehabilitation Engineering*, vol. 15, pp. 327–335, 2007.